research papers

Octahedral tilts, symmetry-adapted displacive modes and polyhedral volume ratios in perovskite structures

Di Wang* and Ross J. Angel

Virginia Tech Crystallography Laboratory, Department of Geosciences, Virginia Polytechnic Institute and State University, Blacksburg, VA 24061, USA

Correspondence e-mail: wangdi@vt.edu

The structures of tilted perovskites in each of the 15 tilt systems have been decomposed into the amplitudes of symmetry-adapted modes in order to provide a clear and unambiguous definition of the tilt angles. A full expression in terms of the mode amplitudes for the ratio of the volumes of the two polyhedra within the perovskite structure for each of the 15 tilt systems is derived, along with more general expressions in terms of either mode amplitudes or tilt angles that can be used to estimate this ratio when the distortions of the octahedra are small.

1. Introduction

The ABX_3 perovskite structure is adopted by minerals of geological importance and many materials with industrial utility. For example, $(Mg,Fe)SiO_3$ perovskite is the predominant phase in the Earth's lower mantle (Ringwood, 1962; Reid & Ringwood, 1975; Liu, 1976; Mao *et al.*, 1977), $BaTiO_3$ and $PbTiO_3$ are important ferroelectrics (*e.g.* Cohen, 1992), and most high-temperature superconductors are derivatives of the perovskite structure (*e.g.* Uher, 1990) with an example of MgC_xNi_3 being an intermetallic perovskite superconductor (He *et al.*, 2001). Understanding the relationship between structure, structural variation and thermodynamic properties in perovskites is therefore of importance and utility in many fields.

The ABX_3 perovskite structure comprises a three-dimensional framework of corner-linked BX_6 octahedra with A cations occupying the cavities within the framework. In the ideal cubic perovskite structure with space group $Pm\bar{3}m$ the A cations are 12-coordinated, forming AX_{12} coordination cuboctahedra. When the A cations are not large enough for the cavities within the framework, the relatively rigid BX_6 octahedra tilt to reduce the size of the cavities occupied by the A cations (Megaw, 1966). Subsequent analysis (*e.g.* Glazer, 1972; Howard & Stokes, 1998, 2002) has shown that there are 15 symmetrically distinct tilt systems in perovskites that can be parameterized in terms of the tilts of the octahedra around the three mutually perpendicular tetrad axes of the cubic structure. The tilts of consecutive octahedra along each of the three axes can either be of the same sign and magnitude, or of opposite sign but the same magnitude. This leads to the description of the thermodynamics of phase transitions involving changes in the tilting patterns in terms of two three-dimensional order parameters representing the two types of tilts along each of these three axes (*e.g.* Howard & Stokes, 2004). Successful analysis of the thermodynamics of perovskite phase transitions involving tilting (Carpenter *et al.*, 2005,

2010; Carpenter, 2007) has demonstrated that the tilt angles around the pseudo-cubic axes are indeed thermodynamic order parameters.

The ratio of the volume of the AX_{12} coordination cub-octahedron to that of the BX_6 octahedron, V_A/V_B, is equal to 5 in the cubic aristotype structure, and decreases with increasing tilting of the octahedra in the hettotype structures (*e.g.* Avdeev *et al.*, 2007). The relative compressibilities and thermal expansivities of the two polyhedra therefore control whether a given perovskite structure becomes more or less tilted with changes in pressure or temperature (Andrault & Poirier, 1991; Zhao *et al.*, 2004; Angel *et al.*, 2005). In particular, because perovskite structures uniformly become less tilted (on average) with increasing temperature, the compressional behavior of the polyhedra determines the phase diagram for tilt transitions in perovskites (Angel *et al.*, 2005). When the BX_6 octahedra are less compressible than the AX_{12} sites the tilts increase with pressure within a single phase, and when tilt transitions occur they do so to structures with greater tilts and lower symmetry, giving the phase transition boundary a positive slope dP/dT. Conversely, when the BX_6 octahedra are softer than the AX_{12} sites, tilting decreases with increasing pressure, and tilt transitions occur to less tilted structures with higher symmetry through a phase transition boundary with dP/dT < 0 (Angel *et al.*, 2005). Thus, the polyhedral volume ratio of perovskites, V_A/V_B, and its change with pressure and temperature, is also an important thermodynamic parameter which must be linked to the values of tilt angles as the primary order parameters for tilt transitions.

Calculation of the tilt angles and the polyhedral volume ratio from experimentally determined perovskite structures is therefore of critical importance for understanding and characterizing the thermodynamics of perovskites. However, except for structures in the three simplest tilt systems and the trivial case of the cubic aristotype, the octahedra are permitted by symmetry to become distorted in such a way that affects the tilt angles and the polyhedral volume ratio. Thomas (1996, 1998) proposed a method to quantitatively describe all perovskite structures by a few length and angle parameters. Three of the angle parameters were defined as the angles between BX_6 octahedral stalks which connect opposite octahedral vertices, and the corresponding closest pseudo-cubic axes. However, these angles do not correspond to the three tilt angles around the pseudo-cubic axes, especially in tilt systems with three tilts, and they include the distortions of the octahedra as well. Tamazyan & van Smaalen (2007) proposed another geometric parameterization of perovskite structures where the orientation of BX_6 octahedra is described by two rotation angles around the z axis and an axis in the xy plane in a direction defined by a third angle. As the orientation of the octahedra is defined by only two rotation axes and the second one is not necessarily the x or y axis, this description is not aimed at the quantification of the tilts around the three pseudo-cubic axes. Furthermore, as illustrated by these two examples, the decomposition of a perovskite structure including tilted and distorted octahedra by geometric analysis does not result in an unambiguous definition of the Glazer

(1972) tilts and the problem is more acute in perovskites with lower space-group symmetries (Avdeev *et al.*, 2007). As a consequence, Avdeev *et al.* (2007) provided expressions for the polyhedral volume ratios as direct functions of the fractional coordinates of the anions in each of the perovskite space groups. However, except for the four simplest cases mentioned above, unambiguous expressions for both the Glazer tilts and their relationship to the V_A/V_B ratio are still to be determined explicitly for each space group, and in a general form.

In this paper we make use of the computer programs *ISOTROPY* (Stokes *et al.*, 2007) and *ISODISTORT* (or the earlier *ISODISPLACE*; Campbell *et al.*, 2006) to analyze perovskite structures in terms of the irreducible representations of the space group of the parent structure (Perez-Mato *et al.*, 2010). Irreducible representations and symmetry-adapted modes provide a clear and unambiguous way to separate the effects of distortion and tilting of octahedra in perovskites because the modes by definition are orthogonal to one another. We decompose the coordinates in the explicit expressions for V_A/V_B in the 15 tilt systems (Avdeev *et al.*, 2007) into symmetry-adapted mode amplitudes, to express V_A/V_B as a direct function of the amplitudes of the modes that measure the octahedral tilts and distortions. A comparison of these expressions reveals a general formula that provides a very close approximation to the value of V_A/V_B for all tilt systems both in terms of the mode amplitudes and the values of the Glazer (1972) tilts.

2. Symmetry-adapted mode analysis of perovskites

2.1. Previous studies

The perovskite structures were first systematically classified by Glazer (1972) according to the different tilting patterns of BX_6 octahedra around the a, b and c axes of the cubic aristotype. Glazer restricted consideration to a simple and common case where the octahedra along the rotation axis rotate by the same angle in the same sense or in opposite senses alternately, which are called 'in-phase' and 'out-of-phase' tilts. By inspecting all combinations of in-phase and out-of-phase tilts around the three pseudo-cubic axes by the same or different angles, Glazer found 23 tilt systems and assigned their space groups accordingly. Each tilt system was denoted by a symbol $a^\# b^\# c^\#$, where # takes 0, + or − if there is no tilt, or in-phase or out-of-phase tilt around the relevant axis. While the analysis by Glazer (1972) greatly assisted in the correct structural analysis of many perovskite systems, it left three crucial issues unaddressed. First were the subtle symmetry issues – whether the tilt systems with higher symmetry between the tilts than required by the space-group symmetry were really distinct tilt systems, and whether some proposed tilt systems actually involved two tilts around a single axis. Second, except in the case of three simple tilt systems $a^- a^- a^-$, $a^0 a^0 c^+$ and $a^0 a^0 c^-$, the calculation of the

values of the tilts from atomic coordinates is neither well defined nor unique. Related to that issue, in the majority of tilt systems in which octahedral distortion is permitted by the space-group symmetry, the separation of distortions and tilts can be done in many ways resulting in different values for the tilt angles.

All three of these issues were addressed by Howard & Stokes (1998, 2002) who followed the description of tilting patterns of perovskite by Glazer (1972) and analysed the tilts in the context of the Landau theory of phase transitions assisted by the computer program *ISOTROPY* (Stokes *et al.*, 2007). The octahedral rotations about the *B* cations are represented by irreducible representations (irreps) whose basis modes are sets of pseudo-vectors at Wyckoff *a* sites where *B* cations are located. Because BX_6 octahedra may tilt in opposite senses alternately along the three pseudo-cubic axes, the unit-cell dimensions of tilted perovskites can be at most doubled compared with that of the cubic aristotype. Thus, only irreps at special k-points Γ $(0, 0, 0)$, X $(0, 0, \frac{1}{2})$, M $(\frac{1}{2}, \frac{1}{2}, 0)$ and R $(\frac{1}{2}, \frac{1}{2}, \frac{1}{2})$ in the reciprocal space of the cubic aristotype need be considered. Of the possible irreps, Howard & Stokes (1998, 2002) showed that the basis modes of two three-dimensional irreps M_3^+ and R_4^+ (notation of Miller & Love, 1967) represent the two types of tilt patterns of the octahedra. The in-phase tilt patterns $b^0b^0a^+$, $a^+b^0b^0$, $b^0a^+b^0$ correspond to the three basis modes of irrep M_3^+, and different combinations of these basis modes generate four tilt systems with only in-phase tilts. Similarly, the three basis modes of irrep R_4^+ correspond to the out-of-phase tilt patterns $b^0b^0a^-$, $a^-b^0b^0$, $b^0a^-b^0$, and in various combinations generate the six tilt systems with only out-of-phase tilts. Coupling of M_3^+ and R_4^+ results in 14 potential tilt systems, four of which belong to the simple case Glazer (1972) considered where in-phase and out-of-phase tilts do not coexist around any individual pseudo-cubic axis. In all, this irrep analysis by Howard & Stokes (1998, 2002) identified 15 tilt systems including the cubic aristotype, all of which were among the 23 tilt systems listed by Glazer. The remaining eight tilt systems listed by Glazer are either a special case of one of the 15 tilt systems or a complex case where in-phase and out-of-phase tilts are allowed by the symmetry to coexist around one pseudo-cubic axis; details are provided by Howard & Stokes (1998, 2002).

Darlington (2002*a*,*b*) and Knight (2009) developed an analysis that is essentially equivalent to that of using irreps, by manually decomposing the tilted perovskite structures in terms of condensed normal modes of the cubic aristotype. By comparing the atomic displacements allowed by the space group of tilted perovskites with the mode displacements associated with X, M and R points, Knight (2009) identified the modes condensed in the 15 tilted perovskite structures. For each of the structures, he found as many modes as the internal degrees of freedom and gave the equation relating the mode amplitudes and the fractional coordinates as well as cell dimensions. The equation for the perovskite structure with $a^+b^-b^-$ tilting and space group *Pbnm* is quoted from Knight (2009) as an example

$$
\begin{pmatrix}
1 & 0 & 0 & 0 & 0 & 0 & 0 \\
0 & 1 & 0 & 0 & 0 & 0 & 0 \\
0 & 0 & 1 & 0 & 0 & 0 & -1 \\
0 & 0 & 0 & 0 & 1 & 0 & 0 \\
0 & 0 & 0 & -1 & 0 & 1 & 0 \\
0 & 0 & 0 & 1 & 0 & 1 & 0 \\
0 & 0 & -1 & 0 & 0 & 0 & -1
\end{pmatrix}
\begin{pmatrix}
d_1 \\ d_2 \\ d_3 \\ d_4 \\ d_5 \\ d_6 \\ d_7
\end{pmatrix}
=
\begin{pmatrix}
au/\sqrt{2} \\
bv/\sqrt{2} \\
au1/\sqrt{2} \\
bv1/\sqrt{2} \\
\sqrt{2}au2 \\
\sqrt{2}bv2 \\
cw2
\end{pmatrix}.
$$

$$(1)$$

The parameters d_i are the mode amplitudes, which is the distance of the independent displacement component of the mode in length units (typically Å or nm). They are dependent upon the a, b and c unit-cell dimensions of the *Pbnm* structure, and the deviations u, v and w of the free fractional coordinates of a set of symmetry-independent atoms from the ideal coordinates corresponding to the cubic aristotype. Among the seven mode amplitudes, d_3 and d_4 correspond to the R_4^+ and M_3^+ modes inducing out-of-phase b^-b^- and in-phase a^+ tilts. Such decompositions explicitly isolate tilting from distortion of the octahedra. The tilt angle around a pseudo-cubic axis can then be calculated by the amplitude of the corresponding octahedral tilt mode

$$
\varphi = \arctan\left(2\left(\frac{N}{V}\right)^{1/3} d\right),
$$

$$(2)$$

where φ is the octahedral tilt angle around a pseudo-cubic axis, d is the amplitude of the M_3^+ or R_4^+ mode associated with the axis, V is the unit-cell volume of the tilted structure, and N is the multiplicity of the unit cell compared with the cubic aristotype (Knight, 2009).

2.2. Mode analysis using *ISOTROPY* and *ISODISTORT*

ISOTROPY (Stokes *et al.*, 2007) can be used to search for displacive modes of A and X atoms in cubic perovskite and provide a comparison with the results of Cowley (1964). Thus, we searched for irreps at k-points X, M and R of space group $Pm\bar{3}m$, carried by modes composed of vectors at Wyckoff b and d sites occupied by A and X atoms. *ISOTROPY* found all the irreps identified by Knight (2009) in the 15 tilted perovskite structures, for which the basis sets of vectors at Wyckoff b or d sites shown by *ISOTROPY* suggest the same basis modes as tabulated in Cowley (1964) and Knight (2009) except for irrep X_5^+. The six basis modes of irrep X_5^+ suggested by *ISOTROPY* are linear combinations of those of Cowley's (Table 1). It can be easily deduced that the matrix describing this linear relationship can also relate, by similarity transformation, the irrep matrix carried by *ISOTROPY*'s basis modes and that carried by Cowley's basis modes, for each symmetry operation in the space group $Pm\bar{3}m$. The two sets of matrices are actually equivalent irreps of X_5^+ according to the group theory. Thus, the broad search for irreps using *ISOTROPY* verifies all the irreps and their basis modes which have been identified by Knight (2009) in the 15 tilted perovskite structures.

Given the parent structure, *ISODISTORT* (Campbell *et al.*, 2006) can decompose a distorted structure with lower

symmetry into symmetry-adapted modes of macroscopic strain, atomic displacement and site occupancy. For each displacive mode condensed in the distorted structure, *ISODISTORT* expresses the displacement directions of affected atoms in terms of the directions in the supercell of the symmetry-independent atoms, and hence can be used to relate the mode amplitudes and the fractional coordinates in a form similar to (1). Note that Knight (2009) incorporates unit-cell dimensions a, b and c into the equations, so the resulting mode amplitudes d_i depend on the cell dimensions. However, *ISODISTORT* describes the superlattice deformation of the distorted structure as macroscopic strain modes, so the displacive modes are referred to the basis of the undeformed superlattice which is an exact transformation of the cubic lattice of the aristotype. Thus, the cell parameter changes of the distorted structure are attributed to the strain modes and the displacive mode amplitudes depend only on fractional coordinates. For the displacive-mode decomposition of perovskites, we can therefore round the cell dimensions a, b and c in (1) to multiples of that of the cubic aristotype a_p and divide both sides of the equation by a_p. After eliminating the coefficients on the right-hand side, we have

$$\begin{pmatrix} 1 & 0 & 0 & 0 & 0 & 0 & 0 \\ 0 & 1 & 0 & 0 & 0 & 0 & 0 \\ 0 & 0 & 1 & 0 & 0 & 0 & -1 \\ 0 & 0 & 0 & 0 & 1 & 0 & 0 \\ 0 & 0 & 0 & -\frac{1}{2} & 0 & \frac{1}{2} & 0 \\ 0 & 0 & 0 & \frac{1}{2} & 0 & \frac{1}{2} & 0 \\ 0 & 0 & -\frac{1}{2} & 0 & 0 & 0 & -\frac{1}{2} \end{pmatrix} \begin{pmatrix} d_1' \\ d_2' \\ d_3' \\ d_4' \\ d_5' \\ d_6' \\ d_7' \end{pmatrix} = \begin{pmatrix} u \\ v \\ u1 \\ v1 \\ u2 \\ v2 \\ w2 \end{pmatrix}, \quad (3)$$

where $d_i' = d_i/a_p$ are clearly the mode amplitudes in terms of only the changes of the fractional coordinates of the atoms within the unit cell of the cubic aristotype, and do not incorporate the unit-cell deformation, so this form of mode decomposition equation follows the separation between strain and displacive modes in *ISODISTORT*.

In fact, the atomic displacement directions in the supercell shown by *ISODISTORT* for each displacive mode just constitute the corresponding column of the square matrix in (3), except *ISODISTORT* defines the directions such that the magnitude of the largest component is equal to 1 or −1. For example, for the M_3^+ mode of X anions condensed in the *Pbnm* perovskite structure, *ISODISTORT* shows that the symmetry-independent $X1$ anion at $(0, 0, \frac{1}{4})$ does not move while the $X2$ anion moves from the ideal position $(\frac{1}{4}, \frac{1}{4}, 0)$ along the $[-1, 1, 0]$ direction in the supercell. However, we cannot simply put these direction components into the fourth column in (3) associated with the M_3^+ mode because the numbers in the column should be the coordinate changes induced by the unit-mode amplitude $d_4' = 1$ or $d_4 = a_p$. The supercell lattice vectors of the *Pbnm* structure are $[1, 1, 0]$, $[-1, 1, 0]$ and $[0, 0, 2]$ in terms of the cubic lattice vectors, so the direction vector $[-1, 1, 0]$ of the $X2$ anion in the supercell is actually vector $[-2, 0, 0]$ in the cubic parent cell. Let us hypothetically assume that the coordinates of the $X2$ anion change by $[-1, 1, 0]$ in the supercell, then the mode amplitude would be $d_4 = Fa_p$, $F = 2$, recalling that Knight (2009) defines the mode amplitude as the

Table 1
Basis modes of irreps M_2^+, M_3^+, R_3^+, R_4^+, R_5^+ and X_5^+ of the space group $Pm\bar{3}m$.

Reproduced from Knight (2009). The mode displacements are derived by Cowley (1964).

Irrep	Wavevector	A cation displacements†	X anion displacements‡
M_2^+	$(0, \frac{1}{2}, \frac{1}{2})$	–	$X_I(z) = -X_{II}(y)$
	$(\frac{1}{2}, 0, \frac{1}{2})$	–	$X_I(z) = -X_{III}(x)$
	$(\frac{1}{2}, \frac{1}{2}, 0)$	–	$X_{III}(x) = -X_{II}(y)$
M_3^+	$(0, \frac{1}{2}, \frac{1}{2})$	–	$X_I(y) = -X_{II}(z)$
	$(\frac{1}{2}, 0, \frac{1}{2})$	–	$X_I(x) = -X_{III}(z)$
	$(\frac{1}{2}, \frac{1}{2}, 0)$	–	$X_{II}(x) = -X_{III}(y)$
R_3^+	$(\frac{1}{2}, \frac{1}{2}, \frac{1}{2})$	–	$X_I(z) = X_{II}(y) = -\frac{1}{2}X_{III}(x)$
			$X_I(z) = -X_{II}(y)$
R_4^+	$(\frac{1}{2}, \frac{1}{2}, \frac{1}{2})$	–	$X_I(y) = -X_{II}(z)$
			$X_I(x) = -X_{III}(z)$
			$X_{II}(x) = -X_{III}(y)$
R_5^+	$(\frac{1}{2}, \frac{1}{2}, \frac{1}{2})$	$A(x)$	$X_I(y) = X_{II}(z)$
		$A(y)$	$X_I(x) = X_{III}(z)$
		$A(z)$	$X_{II}(x) = X_{III}(y)$
X_5^+ (Cowley, 1964)	$(0, \frac{1}{2}, 0)$	$A(z)$	$X_{II}(z)$
		$A(x)$	$X_{II}(x)$
	$(0, 0, \frac{1}{2})$	$A(x)$	$X_I(x)$
		$A(y)$	$X_I(y)$
	$(\frac{1}{2}, 0, 0)$	$A(y)$	$X_{III}(y)$
		$A(z)$	$X_{III}(z)$
X_5^+ (ISOTROPY)	$(0, \frac{1}{2}, 0)$	$A(z) = -A(x)$	$X_{II}(z) = -X_{II}(x)$
		$A(z) = A(x)$	$X_{II}(z) = X_{II}(x)$
	$(0, 0, \frac{1}{2})$	$A(x) = -A(y)$	$X_I(x) = -X_I(y)$
		$A(x) = A(y)$	$X_I(x) = X_I(y)$
	$(\frac{1}{2}, 0, 0)$	$A(y) = -A(z)$	$X_{III}(y) = -X_{III}(z)$
		$A(y) = A(z)$	$X_{III}(y) = X_{III}(z)$

† The A cation is at $(\frac{1}{2}, \frac{1}{2}, \frac{1}{2})$ in the cubic unit cell. ‡ I, II and III are used by Cowley to denote the three X anions at $(0, 0, \frac{1}{2})$, $(0, \frac{1}{2}, 0)$ and $(\frac{1}{2}, 0, 0)$ in the cubic unit cell. The x, y and z in parentheses indicate the displacement direction in the cubic lattice. The mode displacements in other unit cells can be deduced from the wavevector of the mode.

distance of the independent displacement component. Therefore, the direction vector $[-1, 1, 0]$ divided by the factor $F = 2$ are the coordinate changes induced by the unit-mode amplitude and the resulting $-\frac{1}{2}$ and $\frac{1}{2}$ should be put into the fifth and sixth positions of the fourth column associated with $u2 = x_{X2} - \frac{1}{4}$ and $v2 = y_{X2} - \frac{1}{4}$.

Owing to the F factor, and the different terminology used by *ISODISTORT*, the mode amplitude output from *ISODISTORT* must be converted to obtain the mode amplitudes d_i', which otherwise have to be calculated by solving (3). *ISODISTORT* outputs the standard supercell-normalized amplitude As rather than d defined by Knight (2009). Their relationship is $As = (1/normfactor) \times d/(Fa_p)$, where the *normfactor* depends on the structure and Fa_p is the mode amplitude produced by the relevant atoms' direction vectors. With $d' = d/a_p$, we have

$$d' = As \times normfactor \times F. \quad (4)$$

ISODISTORT calculates As and *normfactor* for each displacive mode condensed in the input structure, so in practice we can obtain d_i' of each mode by this simple expression rather than solving (3).

Based on (3) we add the ideal values of the independent fractional coordinates corresponding to the cubic aristotype

research papers

on both sides of the equation, so that the mode amplitudes are directly related to the fractional coordinates. The results for all the 15 tilted perovskite structures are listed in Table S1 of the supplementary material. The space group settings and Wyckoff positions adopted for the 15 perovskite structures follow Table 5 of Woodward (1997) and Table 1 of Avdeev *et al.* (2007), except we use $P\bar{1}$ rather than $F\bar{1}$ because *ISODISTORT* does not accept input structures in space-group settings that are not included in the *International Tables for Crystallography*. In Table S1 we omit the prime symbol for d and use three subscripts. Other than Miller & Love's irrep symbol, the first subscript indicates whether the mode involves displacements of *A* cations at cubic Wyckoff *b* sites or *X* anions at *d* sites. The digits in the third subscript indicate which basis modes of the irrep make up the linear combination acting as one symmetry-adapted mode. We should note that the basis modes constituting the symmetry-adapted mode can change if a different subgroup of $Pm\bar{3}m$ is chosen for the tilted perovskite structure containing the mode, which is conjugate to that used in this study. In this case the symmetry operation in $Pm\bar{3}m$ which relates the two conjugate subgroups transforms the domain state used in this study to another. So, the order parameter for each irrep is multiplied by the matrix representing the operation in the irrep and may become a different combination of basis modes. As an independent component of a varying order parameter, the symmetry-adapted mode may also become a different combination of basis modes of the associated irrep, and hence may be denoted by different digits in the third subscript.

Table 2
V_A/V_B as a function of mode amplitudes for 15 tilted perovskite structures.

The expression of V_A/V_B following the equals sign is in terms of the amplitudes of all the symmetry-adapted modes of *X* anions condensed in each tilted perovskite structure and that following the approximately equal sign is in terms of only the tilt-mode amplitudes. The mode amplitude is a fraction of a_p, the unit-cell dimension of the cubic aristotype. The prime symbol in d' is omitted for tidiness. The three subscripts of d are, in sequence: the relevant atom type, the irrep and the group of digits indicating the linear combination of the corresponding basis modes of the irrep.

a	$a^0a^0a^0$	No. 221 $Pm\bar{3}m$

$$\frac{V_A}{V_B} = 5$$

b	$a^-a^-a^-$	No. 167 $R\bar{3}c$

$$\frac{V_A}{V_B} = \frac{6}{1 + 4 \times 3d^2_{X,R_4^+,123}} - 1$$

c	$a^0a^0c^+$	No. 127 $P4/mbm$

$$\frac{V_A}{V_B} = \frac{6}{1 + 4d^2_{X,M_3^+,1}} - 1$$

d	$a^0a^0c^-$	No. 140 $I4/mcm$

$$\frac{V_A}{V_B} = \frac{6}{1 + 4d^2_{X,R_4^+,1}} - 1$$

e	$a^0b^-b^-$	No. 74 $Imma$

$$\frac{V_A}{V_B} = \frac{6}{1 + 8d^2_{X,R_4^+,12} - 8d^2_{X,R_5^+,12}} - 1$$
$$\simeq \frac{6}{1 + 4 \times 2d^2_{X,R_4^+,12}} - 1$$

f	$a^0b^-c^-$	No. 12 $I2/m$ (non-standard setting of $C2/m$)

$$\frac{V_A}{V_B} = \frac{6}{1 + 4d^2_{X,R_4^+,1} + 4d^2_{X,R_4^+,2} - 4d^2_{X,R_5^+,1} - 4d^2_{X,R_5^+,2}} - 1$$
$$\simeq \frac{6}{1 + 4\left(d^2_{X,R_4^+,1} + d^2_{X,R_4^+,2}\right)} - 1$$

g	$a^-b^-b^-$	No. 15 $I2/a$ (non-standard setting of $C2/c$)

$$\frac{V_A}{V_B} = \frac{6}{1 - 4d^2_{X,R_5^+,12} + 8d^2_{X,R_4^+,13} + 4d^2_{X,R_4^+,2} - 8d^2_{X,R_5^+,13}} - 1$$
$$\simeq \frac{6}{1 + 4\left(2d^2_{X,R_4^+,13} + d^2_{X,R_4^+,2}\right)} - 1$$

h	$a^+b^-b^-$	No. 62 $Pnma$

$$\frac{V_A}{V_B} = \frac{6}{1 - 4d^2_{X,M_2^+,3} + 4d^2_{X,M_3^+,3} + 8d^2_{X,R_4^+,12} - 8d^2_{X,R_5^+,12} + 16\left(d_{X,M_2^+,3} + d_{X,M_3^+,3}\right)\left(d_{X,R_4^+,12} + d_{X,R_5^+,12}\right)d_{X,X_5^+,1}} - 1$$
$$\simeq \frac{6}{1 + 4\left(d^2_{X,M_3^+,3} + 2d^2_{X,R_4^+,12}\right)} - 1$$

i	$a^+a^+c^-$	No. 137 $P4_2/nmc$

$$\frac{V_A}{V_B} = \frac{6}{1 + 8d^2_{X,M_3^+,23} - 4d^2_{X,M_4^+,1} - 8d^2_{X,M_4^+,23} + 4d^2_{X,R_4^+,1} - 16d_{X,M_4^+,1}\left(d^2_{X,M_3^+,23} - d^2_{X,M_4^+,23}\right)} - 1$$
$$- 16\left(d_{X,M_3^+,23} - d_{X,M_4^+,23}\right)d_{X,R_4^+,1}d_{X,X_5^+,1256}$$
$$\simeq \frac{6}{1 + 4\left(2d^2_{X,M_3^+,23} + d^2_{X,R_4^+,1}\right)} - 1$$

Table 2 (continued)

j $a^0b^+c^-$ No. 63 *Cmcm*

$$\frac{V_A}{V_B} = \frac{6}{1 + 4d^2_{X,M_3^+,1} - 4d^2_{X,M_4^+,1} + 4d^2_{X,R_5^+,3} - 4d^2_{X,R_5^+,3} - 8\left(d_{X,M_3^+,1} - d_{X,M_4^+,1}\right)\left(d_{X,R_4^+,3} - d_{X,R_5^+,3}\right)d_{X,X_5^+,34}} - 1$$

$$\simeq \frac{6}{1 + 4\left(d^2_{X,M_3^+,1} + d^2_{X,R_4^+,3}\right)} - 1$$

k $a^+b^-c^-$ No. 11 $P2_1/m$

$$\frac{V_A}{V_B} = \frac{6}{1 + 4d^2_{X,M_1^+,3} - 4d^2_{X,M_2^+,3} + 4d^2_{X,M_3^+,3} - 4d^2_{X,M_4^+,3} + 4d^2_{X,R_4^+,1} + 4d^2_{X,R_4^+,2} - 4d^2_{X,R_5^+,1} - 4d^2_{X,R_5^+,2}}$$

$$+ 8\left(\begin{array}{l}\left(d_{X,M_1^+,3} + d_{X,M_2^+,3} + d_{X,M_3^+,3} + d_{X,M_4^+,3}\right)\left(d_{X,R_4^+,1} + d_{X,R_5^+,1}\right) \\ + \left(d_{X,M_1^+,3} - d_{X,M_2^+,3} - d_{X,M_3^+,3} + d_{X,M_4^+,3}\right)\left(d_{X,R_4^+,2} - d_{X,R_5^+,2}\right)\end{array}\right)d_{X,X_5^+,1}$$

$$- 8\left(\begin{array}{l}\left(d_{X,M_1^+,3} + d_{X,M_2^+,3} - d_{X,M_3^+,3} - d_{X,M_4^+,3}\right)\left(d_{X,R_4^+,1} + d_{X,R_5^+,1}\right) \\ - \left(d_{X,M_1^+,3} - d_{X,M_2^+,3} + d_{X,M_3^+,3} - d_{X,M_4^+,3}\right)\left(d_{X,R_4^+,2} - d_{X,R_5^+,2}\right)\end{array}\right)d_{X,X_5^+,2}$$

$$\simeq \frac{6}{1 + 4\left(d^2_{X,M_3^+,3} + d^2_{X,R_4^+,1} + d^2_{X,R_4^+,2}\right)} - 1$$

l $a^+a^+a^+$ No. 204 $Im\bar{3}$

$$\frac{V_A}{V_B} = \frac{6}{1 + 12d^2_{X,M_3^+,123} - 12d^2_{X,M_4^+,123} + 16\left(3d^2_{X,M_3^+,123} + d^2_{X,M_4^+,123}\right)d_{X,M_4^+,123}} - 1$$

$$\simeq \frac{6}{1 + 4 \times 3d^2_{X,M_3^+,123}} - 1$$

m $a^0b^+b^+$ No. 139 $I4/mmm$

$$\frac{V_A}{V_B} = \frac{6}{1 + 8d^2_{X,M_3^+,23} - 4d^2_{X,M_4^+,1} - 8d^2_{X,M_4^+,23} - 16d_{X,M_4^+,1}\left(d^2_{X,M_3^+,23} - d^2_{X,M_4^+,23}\right)} - 1$$

$$\simeq \frac{6}{1 + 4 \times 2d^2_{X,M_3^+,23}} - 1$$

n $a^+b^+c^+$ No. 71 *Immm*

$$\frac{V_A}{V_B} = \frac{6}{1 + 4d^2_{X,M_3^+,1} + 4d^2_{X,M_3^+,2} + 4d^2_{X,M_3^+,3} - 4d^2_{X,M_4^+,1} - 4d^2_{X,M_4^+,2} - 4d^2_{X,M_4^+,3}}$$

$$+ 16d_{X,M_3^+,3}\left(d_{X,M_3^+,2}d_{X,M_4^+,1} + d_{X,M_3^+,1}d_{X,M_4^+,2}\right)$$

$$+ 16\left(d_{X,M_3^+,1}d_{X,M_3^+,2} + d_{X,M_4^+,1}d_{X,M_4^+,2}\right)d_{X,M_4^+,3}$$

$$\simeq \frac{6}{1 + 4\left(d^2_{X,M_3^+,1} + d^2_{X,M_3^+,2} + d^2_{X,M_3^+,3}\right)} - 1$$

o a^-b^-c- No. 2 $P\bar{1}$

$$\frac{V_A}{V_B} = \frac{6}{1 + 12d^2_{X,R_1^+,1} - 3d^2_{X,R_3^+,1} - 4d^2_{X,R_3^+,2} + 4d^2_{X,R_4^+,1} + 4d^2_{X,R_4^+,2} + 4d^2_{X,R_4^+,3} - 4d^2_{X,R_5^+,1} - 4d^2_{X,R_5^+,2} - 4d^2_{X,R_5^+,3}} - 1$$

$$\simeq \frac{6}{1 + 4\left(d^2_{X,R_4^+,1} + d^2_{X,R_4^+,2} + d^2_{X,R_4^+,3}\right)} - 1$$

---

and $P112_1/m$ in Knight, 2009) structures, rather than the R_5^+ basis modes themselves such as $A(x)$, $A(y)$, $A(z)$ in the $P\bar{1}$ ($F\bar{1}$ in Knight, 2009) structure. In these three structures, whether the R_5^+ basis modes or their linear combinations are used affects the relevant part of the mode decomposition equation. The second point is similar; that in the $P2_1/m$ structure the linear combinations of X_5^+ basis modes $X_I(x) = X_I(y)$ and $X_I(x) = -X_I(y)$ *ISODISTORT* uses mean that the mode decomposition equation is a little different from Knight's which involves the X_5^+ basis modes $X_I(x)$ and $X_I(y)$. The third point is that although Knight did not write the R_3^+ mode in the $I2/a$ ($I2_1/b11$ in Knight, 2009) perovskite structure as a linear combination of basis modes $X_I(z) = X_{II}(y) = -\frac{1}{2}X_{III}(x)$ and $X_I(z) = -X_{II}(y)$ of irrep R_3^+ (Table 1), the mode he wrote as $X_{II}(y) = -X_{III}(x)$ is actually a linear combination of the two basis modes as denoted by our symbol $d_{X,R_3^+,12}$ (Table S1*g*). However, if the space group $I2/a$ undergoes a conjugate subgroup transformation (as mentioned previously) through the threefold rotation around the cubic $[1, 1, 1]$ direction C_{31}^+, the mode $X_{II}(y) = -X_{III}(x)$ would transform to $X_I(z) = -X_{II}(y)$, the second basis mode of irrep R_3^+, and hence the symbol would be $d_{X,R_3^+,2}$ rather than $d_{X,R_3^+,12}$. This is an example of the mode symbol changing with the domain states described by different conjugate subgroups of $Pm\bar{3}m$.

3. Polyhedral volume ratio V_A/V_B

3.1. V_A/V_B as a function of displacive mode amplitudes

Avdeev *et al.* (2007) derived the formulae for the AX_{12} and BX_6 polyhedral volume ratio V_A/V_B in terms of the fractional coordinates of the X anions for the 15 tilted perovskite structures and the $Pm\bar{3}m$ aristotype structure. Note that the

unit-cell parameters do not appear in the formulae because although they affect the values of V_A and V_B, changes in the unit-cell parameters change both polyhedral volumes in the same proportion and the ratio V_A/V_B therefore remains unaffected by the unit-cell parameters. Further, because the AX_{12} cuboctahedra and BX_6 octahedra are bound by X anions, the V_A/V_B formulae only contain the fractional coordinates of the X anions. If we substitute the lines concerning the X anions in the mode decomposition equation into the V_A/V_B formula of Avdeev *et al.* (2007), we can obtain the V_A/V_B formula in terms of the amplitudes of the displacive modes of the X anions. The resulting V_A/V_B formulae for the 15 perovskite structures are shown in Table 2. In the *Cmcm*, *I4/mmm*, *P2₁/m*, *P4₂/nmc*, *Im3̄* and *Immm* structures, the A or B cation occupies more than one symmetry-independent site and hence has more than one polyhedral volume, as denoted in Table 1 of Avdeev *et al.* (2007). In these cases, the expression for the ratio of the average polyhedral volumes is used for substitution. As expected, only the modes involving the X anions are present in the formulae. All the formulae have a common general form in which if all the mode amplitudes in the denominator are zero, V_A/V_B becomes 5, the value in the cubic aristotype structure without any distortion. V_A/V_B can become smaller or larger than 5 depending on the mode amplitudes. We should note that the V_A/V_B formulae given in Table 2 are based on the mode-decomposition equations given in Table S1. If we substitute a mode amplitude d' with $-d'$ in the mode decomposition equation, the resulting V_A/V_B formula would also have the d' replaced by $-d'$.

3.2. Effect of octahedral tilt modes on V_A/V_B

Of all the displacive modes of the X anions, the M_3^+ and R_4^+ modes can induce in-phase and out-of-phase octahedral tilts, and hence are called octahedral tilt modes. The other modes only contribute to the distortion of the octahedra and hence are called octahedral distortion modes. We should emphasize that even in the absence of octahedral distortion modes it is possible for the octahedra to be distorted as a consequence of the deviation of the metric from cubic symmetry. These types of distortions are therefore included in the Γ-point strain modes and not in the octahedral distortion modes.

If we keep only the octahedral tilt modes in the V_A/V_B formula and set the octahedral distortion modes to zero, we can obtain the V_A/V_B formula as a function of the amplitudes of the octahedral tilt modes alone. The results for the 15 tilted perovskite structures are shown in Table 2 and are indicated by the use of 'approximately equal' signs. The resulting formulae are much simpler and have the general form

$$\frac{V_A}{V_B} = \frac{6}{1 + 4\sum_i n_i d_i'^2} - 1, \qquad (5)$$

where the sum is over all of the condensed octahedral tilts (at most three modes in all tilted perovskite structures), d_i' is the amplitude of the ith octahedral tilt mode which is a linear combination of the basis modes of irrep M_3^+ or R_4^+, and n_i is

the number of basis modes involved in the ith mode. Note that the simplified form given in (5) shows that when only the octahedral tilt modes condense, V_A/V_B is never greater than 5 and it decreases with increasing mode amplitudes, in accordance with the experimental observation that the polyhedral volume ratio V_A/V_B can be reduced by octahedral tilting (*e.g.* Thomas & Beitollahi, 1994; Thomas, 1996, 1998; Angel *et al.*, 2005).

The octahedral tilt modes condensed in each tilted perovskite structure coincide with the tilt system. For example, in the structure with $a^+b^-b^-$ tilting and space group *Pnma*, the M_3^+ and R_4^+ modes are condensed with order parameters $(0, 0, d_{X,M_3^+,3})$ and $(d_{X,R_4^+,12}, -d_{X,R_4^+,12}, 0)$, which correspond to the in-phase tilt a^+ and the two out-of-phase tilts b^-b^-. If we denote the amplitudes of the basis modes, of either irrep M_3^+ or R_4^+, associated with a, b and c pseudo-cubic axes as d_a, d_b and d_c, then we have $d_a = d_{X,M_3^+,3}$, $d_b = d_{X,R_4^+,12}$, $d_c = -d_{X,R_4^+,12}$ and equation (5) for $a^+b^-b^-$ (Table 2h) can be rewritten as

$$\frac{V_A}{V_B} = \frac{6}{1 + 4(d_a^2 + d_b^2 + d_c^2)} - 1. \qquad (6)$$

It is straightforward to test this form for the rest of the 15 tilt systems.

Recall equation (2) showing the relationship between the octahedral tilt angle around a pseudo-cubic axis and the corresponding octahedral tilt mode. Since we attribute the unit-cell deformation of the tilted structure to the strain modes, as in *ISODISTORT*, the unit-cell volume can be rounded to the multiple of that of the cubic aristotype, $V = Na_p^3$. Then, equation (2) becomes

$$\varphi = \arctan 2d', \qquad (7)$$

where $d' = d/a_p$ is just one of d_a, d_b and d_c. If we substitute (7) into (6) three times, we have

$$\frac{V_A}{V_B} = \frac{6}{1 + \tan^2 \varphi_a + \tan^2 \varphi_b + \tan^2 \varphi_c} - 1, \qquad (8)$$

where φ_a, φ_b and φ_c are the octahedral tilt angles around a, b and c pseudo-cubic axes, respectively. Thus, after neglecting the unit-cell deformation of the tilted structure (which does not affect V_A/V_B) and all the octahedral distortion modes, the polyhedral volume ratio V_A/V_B becomes a simple function of the octahedral tilt mode amplitudes or the octahedral tilt angles associated with the three pseudo-cubic axes.

For tilt systems involving a tilt about a single axis equation (8) reduces to $V_A/V_B = 6/(1 + \tan^2\varphi) - 1$, which is identical to the more common form of $V_A/V_B = 6\cos^2\varphi - 1$. The latter can be derived by simple geometry and is a special case of $V_A/V_B = 6\cos^2\theta_m\cos\theta_z - 1$ proposed by Thomas (1996) for orthorhombic and tetragonal perovskites, where because the octahedra only rotate around the z axis, the angle between the z axis and the corresponding octahedral stalk θ_z is zero and the other two axis-stalk angles, and hence their average θ_m is equal to the tilt angle φ. For the $a^-a^-a^-$ and $a^+a^+a^+$ tilt systems where the three tilt angles and the three mode amplitudes are equal (*i.e.* $\varphi_a = \varphi_b = \varphi_c = \varphi$ and $d_a = d_b = d_c = d'$) equation (8) reduces to $V_A/V_B = 6/(1 + 3\tan^2\varphi) - 1 = 6/(1 + 12d'^2) - 1$. The

rotation angle ω of the octahedra around the $[1, 1, 1]$ axis can be derived as $\tan \omega = 2\sqrt{3}d'$ from the displacements of the octahedral vertices, so by substitution we obtain $V_A/V_B = 6\cos^2\omega - 1$, which was proposed by Thomas & Beitollahi (1994) for rhombohedral perovskites.

3.3. Geometric proof

Although equation (6) emerges by inspection of the V_A/V_B formulae for all the 15 tilt systems, it can actually be proven quite simply by geometry. Consider the BX_6 octahedron centered at the origin of the unit cell of the cubic aristotype. We use X_a, X_b and X_c to denote the three X anions with the fractional coordinates $(\frac{1}{2}, 0, 0)$, $(0, \frac{1}{2}, 0)$ and $(0, 0, \frac{1}{2})$. The basis mode, of either irrep M_3^+ or R_4^+, associated with the a axis, imposes on X_b and X_c displacements $(0, 0, d_a)$ and $(0, -d_a, 0)$. Similarly, the basis mode associated with the b axis imposes on X_c and X_a displacements $(d_b, 0, 0)$ and $(0, 0, -d_b)$, respectively, and that associated with the c axis imposes on X_a and X_b displacements $(0, d_c, 0)$ and $(-d_c, 0, 0)$. If the octahedral distortion modes are not considered, X_a, X_b and X_c are moved by a combination of all three modes to $(\frac{1}{2}, d_c, -d_b)$, $(-d_c, \frac{1}{2}, d_a)$ and $(d_b, -d_a, \frac{1}{2})$. The volume of the tetrahedron bound by X_a, X_b, X_c and the origin O can be calculated as

$$V_{OX_aX_bX_c} = \frac{1}{6} \cdot \begin{vmatrix} \frac{1}{2} & -d_c & d_b \\ d_c & \frac{1}{2} & -d_a \\ -d_b & d_a & \frac{1}{2} \end{vmatrix} = \frac{1 + 4(d_a^2 + d_b^2 + d_c^2)}{48}, \quad (9)$$

where all lengths are fractions of a_p and the volume is a fraction of a_p^3. The remaining three X anions of the BX_6 octahedron centered at the origin are just related by inversion through the origin to X_a, X_b and X_c. The volumes of these other seven tetrahedra making up the octahedron can be calculated by a determinant as equation (9) and the results are all equal to $V_{OX_aX_bX_c}$. Therefore, the octahedral volume is eight times $V_{OX_aX_bX_c}$ and is the same for all of the other octahedra in the supercell of the tilted perovskite. The volume of the AX_{12} cuboctahedra V_A can be obtained by subtracting the octahedral volume V_B from the total volume a_p^3 associated with each cubic lattice point and the polyhedral volume ratio V_A/V_B can be calculated by

$$\frac{V_A}{V_B} = \frac{1 - 8 \times V_{OX_aX_bX_c}}{8 \times V_{OX_aX_bX_c}} = \frac{6}{1 + 4(d_a^2 + d_b^2 + d_c^2)} - 1, \quad (10)$$

which is just equation (6). Although this result is obtained in reference to the cubic lattice, it applies to all tilted perovskites because, as noted above, the deformation of the unit cell has no effect on the volume ratio V_A/V_B.

4. Worked example with ISODISTORT

As an example of how to extract the information required to calculate the mode amplitudes and tilt angles from *ISODIS-TORT*, we use the room-pressure structure of pure $MgSiO_3$ *Pnma* perovskite published by Dobson & Jacobsen (2004). The original structure was published in the space group *Pbnm*,

Table 3
CIF files for the example calculation in §4.

The items with the name '_space_group_symop_operation_xyz' in the CIF file are needed by *ISODISTORT*. They are omitted here to save space.

Distorted structure
data_MgSiO3_Pnma_P0_DobsonJacobsen
_space_group_name_H-M_alt   'P n m a'
_diffrn_ambient_pressure   0

```
_cell_length_a        4.9298(3)
_cell_length_b        6.8990(3)
_cell_length_c        4.7780(2)
_cell_angle_alpha    90.0000
_cell_angle_beta     90.0000
_cell_angle_gamma    90.0000
```

```
loop_
  _atom_site_label
  _atom_site_fract_x
  _atom_site_fract_y
  _atom_site_fract_z
```

```
Mg  0.55588   0.25000   0.01378
Si  0.00000   0.00000   0.00000
O1 -0.03355   0.25000  -0.10189
O2  0.79867   0.05258   0.30374
```

Parent structure
data_MgSiO3_Pm_3m_P0
_space_group_name_H-M_alt   'P m -3 m'
_diffrn_ambient_pressure   0

```
_cell_length_a        3.438
_cell_length_b        3.438
_cell_length_c        3.438
_cell_angle_alpha    90.0000
_cell_angle_beta     90.0000
_cell_angle_gamma    90.0000
```

```
loop_
  _atom_site_label
  _atom_site_fract_x
  _atom_site_fract_y
  _atom_site_fract_z
```

```
Mg  0.50000   0.50000   0.50000
Si  0.00000   0.00000   0.00000
O   0.50000   0.00000   0.00000
```

so the first step is to transform the published atom coordinates into *Pnma*. Comparison of the resulting coordinates with those given in Table S1*h* for *Pnma* shows that in addition an origin shift has to be applied to place the B cation site (Si) at the origin, and that the O atoms then have to be moved to equivalent positions by the space-group operators so that they correspond exactly to those positions listed in Table S1*h*. The resulting coordinate list is given in Table 3. The cubic perovskite structure never becomes stable under any conditions for $MgSiO_3$, so a fictitious structure has to be constructed to act as a parent reference structure for the *ISODISTORT* program. Note that although the individual values of *As* and *normfactor* produced by *ISODISTORT* depend on the cell parameter of the cubic parent structure, their product used in equation (4) does not. The only requirement is that the volume strain between the parent structure and the distorted structure is sufficiently small to allow *ISODISTORT* to iden-

Table 4
Output from *ISODISTORT*: mode details for the perovskite structure defined in Table 3.

Mode†	As	normfactor	Atom	dx	dy	dz	F factor	d'
R_4^+ $(a,-a,0)$	1.42368	0.07272	O2	0.0	0.5	0.0	1	0.10353
			O1	0.0	0.0	−1.0		
R_5^+ $(a,a,0)$	0.02248	0.07272	O2	0.0	0.5	0.0	1	0.00163
			O1	0.0	0.0	1.0		
X_5^+ $(a,0,0,0,0)$	0.32624	0.10284	O2	0.0	0.0	0.0	1	0.03355
			O1	−1.0	0.0	0.0		
M_2^+ $(0,0,a)$	0.04930	0.05142	O2	−1.0	0.0	1.0	2	0.00507
			O1	0.0	0.0	0.0		
M_3^+ $(0,0,a)$	0.99585	0.05142	O2	1.0	0.0	1.0	2	0.10241
			O1	0.0	0.0	0.0		

† Only those modes involving oxygen displacements are listed in this table. The order parameter for each mode is in the parenthesis.

tify the equivalent atoms, and this can be achieved by setting the unit-cell volume of the cubic parent structure equal to the subcell volume of the distorted structure (Table 3).

After loading the structures to *ISODISTORT*, and performing the mode decomposition (Method 4 for the search) with the appropriate basis (in this case [1, 0, −1],[0, 2, 0],[1, 0, 1]), all of the information required for the calculation of mode amplitudes, tilt angles and the polyhedral volume ratios is provided on the 'modes details' page. The values of *As* and *normfactor* for the modes involving only the O atoms can be copied directly (Table 4). The *F* factors have to be calculated by transforming the displacive mode direction vectors back into the parent subcell. For example, for the O2 atom under the R_4^+ mode, the mode direction vector [dx, dy, dz] is given as [0.0, 0.5, 0.0] in the supercell, which is equivalent to 0.5 times the basis vector [0, 2, 0] in the parent cubic cell, and is thus [0, 1, 0]. As this is a simple lattice vector, the *F* factor is 1. As it should be, the same result is obtained for R_4^+ if the O1 atom is considered; [dx, dy, dz] = [0, 0, −1] so in the parent cubic cell this is equal to −1 × [1, 0, 1] and thus [−1, 0, −1], another simple lattice vector. The *F* factor for the M_3^+ mode is equal to 2, because for O2 [dx, dy, dz] is given as [1, 0, 1] in the distorted structure, and is thus equal to [1, 0, −1] + [1, 0, 1] in the parent cubic structure or [2, 0, 0] which is twice the cubic lattice vector. All of the displacive mode definitions and *F* factors for the example are listed in Table 4.

By inserting the mode amplitudes into the equations listed in Table 2(h), the polyhedral volume ratio for this $MgSiO_3$ perovskite structure is calculated as 4.29, but 4.32 when only the tilt modes are considered. The tilt angles can also now be calculated using equation (7) as $\varphi_a = \arctan(2d_{X,M_3^+,3}) = 11.6°$ and $\varphi_b = \varphi_c = \arctan(2d_{X,R_4^+,12}) = 11.7°$.

5. Experimental data analysis

Review of the expressions given in Table 2 for the polyhedral volume ratio V_A/V_B reveals three distinct classes in terms of the relationship to the mode amplitudes. In this section we review selected experimental data for one example from each of these three classes in order to demonstrate how the inter-

play between the octahedral tilt modes and the octahedral distortion modes controls the variation of the polyhedral volume ratio in each case.

5.1. Perovskites without octahedral distortion

There are three tilt systems, apart from the trivial untilted case of $Pm\bar{3}m$ symmetry, in which no octahedral distortion modes are allowed: $a^-a^-a^-$ ($R\bar{3}c$), $a^0a^0c^+$ ($P4/mbm$) and $a^0a^0c^-$ ($I4/mcm$). The $R\bar{3}c$ perovskite structure is produced by three out-of-phase tilts of equal magnitude around the three pseudo-cubic axes. Correspondingly, the out-of-phase tilt R_4^+ mode condensed in the $R\bar{3}c$ structure is a linear combination of the three R_4^+ basis modes with equal magnitude coefficients. The R_4^+ mode amplitude is thus the only internal degree of freedom. The expression for V_A/V_B in terms of the mode amplitude is therefore a simple function of the tilt mode amplitude alone, as it is for the tilt systems $a^0a^0c^+$ and $a^0a^0c^-$ (Tables 2b–d). For all of these three tilt systems there is a unique relationship between increasing amplitude of the tilt mode and decreasing V_A/V_B ratio.

As an example of a purely tilted perovskite, we considered $LaCrO_3$ perovskite above its orthorhombic to rhombohedral phase transition at approximately 533 K (Hashimoto *et al.*, 2000). The rhombohedral structure with space group $R\bar{3}c$ was determined by neutron powder diffraction up to 1013 K (Oikawa *et al.*, 2000). We calculated the polyhedral volume ratio V_A/V_B from the only free coordinate x_O in the hexagonal unit cell at each temperature using the formula from Avdeev *et al.* (2007), and the mode amplitude $d_{X,R_4^+,123}$ from *ISODISTORT* following equation (4). Fig. 1 shows that the $LaCrO_3$
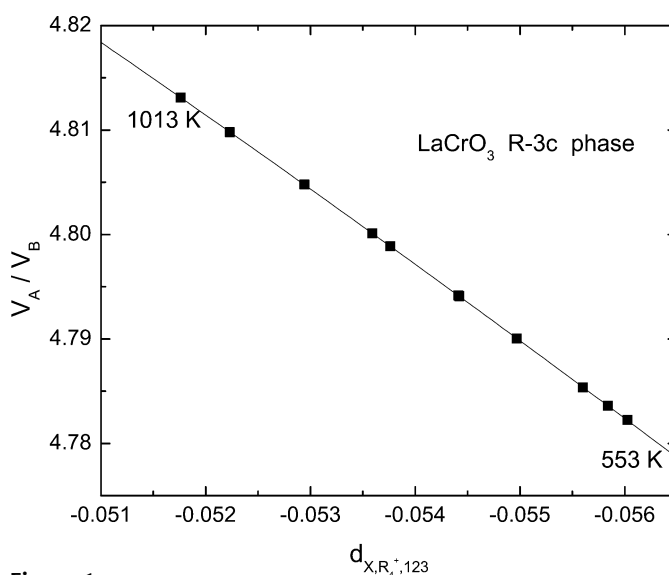

Figure 1
Variation of V_A/V_B calculated from the atomic coordinates (Avdeev *et al.*, 2007) with mode amplitude $d_{X,R_4^+,123}$ of the $R\bar{3}c$ phase of $LaCrO_3$ perovskite. The curve is the V_A/V_B $(d_{X,R_4^+,123})$ expression for the $R\bar{3}c$ structure given in Table 2(b).

experimental data fall on the curve representing the theoretical relationship between the two given in Table 2(b). As the temperature increases, the octahedral tilt mode amplitude $d_{X,R_4^+,123}$ decreases and the polyhedral volume ratio V_A/V_B increases towards 5, both showing that, as normal for $R\bar{3}c$ perovskite structures, LaCrO$_3$ becomes less tilted at higher temperatures and may eventually transform to the aristotype with $Pm\bar{3}m$ symmetry (e.g. Hofer & Kock, 1993).

5.2. Perovskites with separated tilts and distortions.

The *Imma* perovskite structure is produced by $a^0b^-b^-$ tilting which is composed of two out-of-phase tilts around two pseudo-cubic axes by an equal angle and no tilt around the third axis. Correspondingly, the out-of-phase tilt R_4^+ mode condensed in the *Imma* structure is a linear combination of two of the three R_4^+ basis modes with equal magnitude coefficients. There is also an octahedral distortion R_5^+ mode which is a linear combination of two of the three R_5^+ basis modes. The V_A/V_B $(d_{X,R_4^+,12}, d_{X,R_5^+,12})$ expression for the *Imma* structure (Table 2e) is plotted as a surface in Fig. 2, which shows that

V_A/V_B decreases with the octahedral tilt mode amplitude $d_{X,R_4^+,12}$ while it increases with the octahedral distortion mode amplitude $d_{X,R_5^+,12}$. The curve in the $d_{X,R_5^+,12} = 0$ plane just displays the decreasing function $V_A/V_B (d_{X,R_4^+,12})$ omitting the octahedral distortion mode amplitude $d_{X,R_5^+,12}$. This same form of complete separation of the influence of the tilt modes and distortion modes on V_A/V_B is also displayed by two other tilt systems, $a^0b^-c^-$ (*I2/m*) and $a^-b^-b^-$ (*I2/a*) (Table 2f and g). In all three cases the octahedral distortions always contribute to an increase in V_A/V_B, as shown in Fig. 2.

There are limited experimental data for *Imma* perovskites because they normally only exist as an intermediate phase with a limited temperature range of stability (e.g. Howard et al., 2000), although BaPbO$_3$ (Fu et al., 2005, 2007) appears to be an exception. Experimental structural data of several *Imma* perovskites were added to the coordinate frame in Fig. 2. As for the experimental data in Fig. 1, V_A/V_B values in Fig. 2 were calculated from the X anion coordinates following the formula from Avdeev et al. (2007). The mode amplitudes $d_{X,R_4^+,12}$ and $d_{X,R_5^+,12}$ were calculated from *ISODISTORT*. In Fig. 2 the experimental points lie on the theoretical surface from Table 2(e) and hence validate the V_A/V_B expression for the *Imma* structure. Note that the series of experimental points are very close to the $d_{X,R_5^+,12} = 0$ plane, which shows that in real *Imma* perovskite structures the octahedral distortion mode amplitude $d_{X,R_5^+,12}$ is very small compared with the octahedral tilt mode amplitude $d_{X,R_4^+,12}$. Therefore, a good approximation would be to omit $d_{X,R_5^+,12}$ when calculating V_A/V_B of an *Imma* structure. For the compositions where experimental data are available over a range of temperatures the octahedral tilt mode amplitude $d_{X,R_4^+,12}$ decreases with increasing temperature. However, while the octahedral distortion mode amplitude $d_{X,R_5^+,12}$ decreases with increasing temperature in some cases, such as BaCe$_{0.8}$Zr$_{0.2}$O$_3$ and BaTbO$_3$ (Pagnier et al., 2000; Fu et al., 2004), in others such as in SrSnO$_3$ (Goodwin et al., 2007) it increases (Fig. 2). Nonetheless, the change in tilt-mode
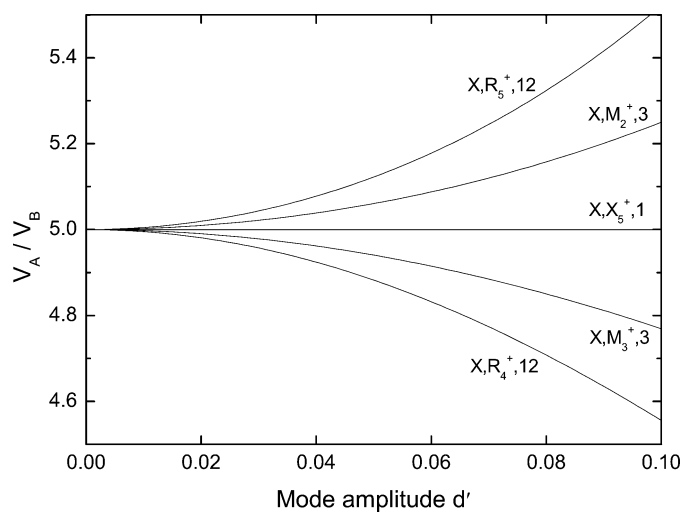

Figure 2
Variation of V_A/V_B with mode amplitudes $d_{X,R_4^+,12}$ and $d_{X,R_5^+,12}$ of *Imma* perovskites. The surface is the V_A/V_B $(d_{X,R_4^+,12}, d_{X,R_5^+,12})$ expression for the *Imma* structure given in Table 2(e). The series of dots are BaPbO$_3$ at 4.2–553 K (red; Fu et al., 2005, 2007), BaCe$_{0.8}$Zr$_{0.2}$O$_3$ at 300 and 345 K (orange; Pagnier et al., 2000), SrSnO$_3$ at 650–790 K (cyan; Goodwin et al., 2007), BaTbO$_3$ at 40–260 K (yellow; Fu et al., 2004), Sr$_{1-x}$Ce$_x$MnO$_3$, x = 0.35, 0.40 (purple; Kennedy et al., 2008), (Na$_{0.5}$Nd$_{0.5}$)$_{1-x}$Sr$_x$TiO$_3$, x = 0.3, 0.4 (green; Ranjan et al., 2006). The black dots are Sr$_{0.6}$Ba$_{0.4}$SnO$_3$ (Mountstevens et al., 2003), CeAlO$_3$ at 373 K (Fu & Ijdo, 2006), BaCeO$_3$ at 573 K (Knight, 1994), PrAlO$_3$ at 185 K (Carpenter et al., 2005), Ca$_{0.4}$La$_{0.4}$TiO$_3$ (Zhang et al., 2007), BaPrO$_3$ at 573 K (Saines et al., 2009), Pr$_{0.76}$La$_{0.24}$AlO$_3$ at 170 K (Basyuk et al., 2009), BaCe$_{0.80}$Y$_{0.20}$O$_{2.9}$ at 773 K (Malavasi et al., 2008), BaPr$_{0.9}$Y$_{0.1}$O$_{3-\delta}$ at 573 K (Knee et al., 2009), 0.3La(Mg$_{0.5}$Ti$_{0.5}$)O$_3$–0.7SrTiO$_3$ (Avdeev et al., 2002) and SrMoO$_3$ at 5 K (Macquart et al., 2010).

Figure 3
Variation of V_A/V_B of the *Pnma* perovskite with individual mode amplitudes $d_{X,M_2^+,3}$, $d_{X,M_3^+,3}$, $d_{X,R_4^+,12}$, $d_{X,R_5^+,12}$ or $d_{X,X_5^+,1}$.

amplitude is greater in all cases so that V_A/V_B increases with increasing temperature as required for the general evolution of the structure towards a higher-symmetry, less tilted polymorph.

5.3. Perovskites with combined tilts and distortions

Seven of the remaining eight tilt systems have expressions for the volume ratio V_A/V_B that contain three types of terms in the denominator (Table 2h–n). In addition to the separate terms in the squares of the individual amplitudes of the tilt and distortion modes found, for example, for *Imma*, the expressions for these tilt systems include third-order products of the amplitudes of both types of modes. As a consequence, the volume ratio of these perovskites can be either larger or smaller than the V_A/V_B ratio due to tilting alone. The last case, of tilt system $a^-b^-c^-$ ($P\bar{1}$), does not contain these triplets, but terms with different signs that can also lead to the distortional modes increasing or decreasing V_A/V_B (Table 2o).

The *Pnma* perovskite structure is the most commonly found tilt system in perovskites. It is produced by $a^+b^-b^-$ tilting which is composed of one in-phase tilt around a pseudo-cubic axis and two out-of-phase tilts around the other two pseudo-cubic axes by an equal angle. Correspondingly, condensed in the *Pnma* structure is an in-phase tilt M_3^+ basis mode and an out-of-phase tilt R_4^+ mode which is a linear combination of two of the three R_4^+ basis modes with equal magnitude coefficients. In addition, there are three octahedral distortion modes: an M_2^+ basis mode, a linear combination of two R_5^+ basis modes and an X_5^+ basis mode (Table 1). The *Pnma* structure thus has a five-variable function for V_A/V_B. The volume ratio as a function of each individual mode amplitude can be obtained simply by making the other four variables zero. The resulting five single-variable functions plotted in Fig. 3 show that V_A/V_B decreases with the octahedral tilt mode amplitudes $d_{X,M_3^+,3}$ and $d_{X,R_4^+,12}$ and increases with the octahedral distortion mode amplitudes $d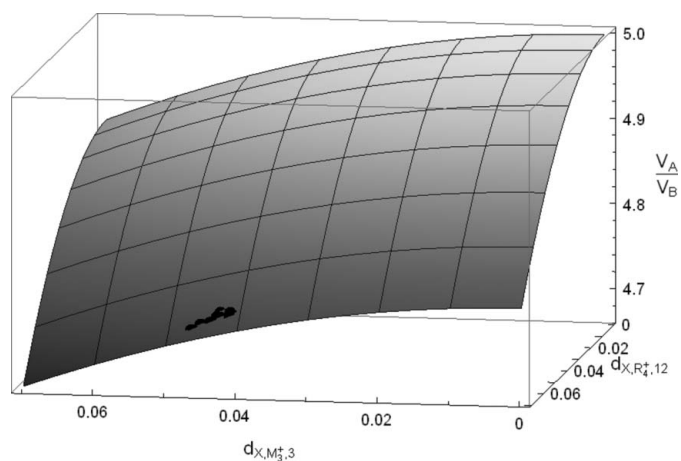_{X,M_2^+,3}$ and $d_{X,R_5^+,12}$. Note that the mode amplitudes $d_{X,R_4^+,12}$ and $d_{X,R_5^+,12}$ change V_A/V_B faster than $d_{X,M_2^+,3}$ and $d_{X,M_3^+,3}$ because they both control two basis modes simultaneously. This is obvious when V_A/V_B is plotted as a function of the two octahedral tilt mode amplitudes $d_{X,M_3^+,3}$ and $d_{X,R_4^+,12}$ in the absence of distortion (Fig. 4), in which the curves in the $d_{X,R_4^+,12} = 0$ and $d_{X,M_3^+,3} = 0$ planes are the same as the curves for $d_{X,M_3^+,3}$ and $d_{X,R_4^+,12}$ in Fig. 3.

The X_5^+ distortional mode is a special case in this respect. It only appears in the four tilt systems that involve both in-phase and out-of-phase tilts because it is associated with the X point in the Brillouin zone. As a consequence its amplitude only appears in product terms with other modes in the expression for the volume ratio V_A/V_B and only in tilt systems $a^+b^-b^-$ (*Pnma*), $a^+a^+c^-$ (*P4$_2$/nmc*), $a^0b^+c^-$ (*Cmcm*) and $a^+b^-c^-$ (*P2$_1$/m*) (Tables 2h–k). Therefore, this mode *alone* does not change the volume ratio V_A/V_B away from 5. Conversely, when the amplitude of the X_5^+ mode in *Pnma* perovskite is zero, the third-order terms in the expression for V_A/V_B are zero and the expression reduces to the form discussed in §5.2, so that the polyhedral volume ratio is increased by the other distortional modes from that given by the tilts alone (Table 2h).

In real *Pnma* perovskites all of the symmetry-allowed modes have non-zero amplitudes, and the effect of the distortional modes on the value of the volume ratio V_A/V_B depends on a subtle balance between the terms in the squares of the distortion mode amplitudes $d_{X,M_2^+,3}$ and $d_{X,R_5^+,12}$ alone and the third-order product terms. As an example of the more common case in *Pnma* perovskites, we use LaCrO$_3$ perovskites once more but at temperatures below the orthorhombic to rhombohedral phase transition temperature at 533 K (Hashimoto *et al.*, 2000). The five mode amplitudes $d_{X,M_2^+,3}$, $d_{X,M_3^+,3}$, $d_{X,R_4^+,12}$, $d_{X,R_5^+,12}$ and $d_{X,X_5^+,1}$ were calculated with *ISODISTORT* for the structures down to 295 K determined by neutron powder diffraction (Oikawa *et al.*, 2000). The results plotted in Fig. 5 show that the two octahedral tilt-mode amplitudes $d_{X,M_3^+,3}$ and $d_{X,R_4^+,12}$ are significantly larger than the
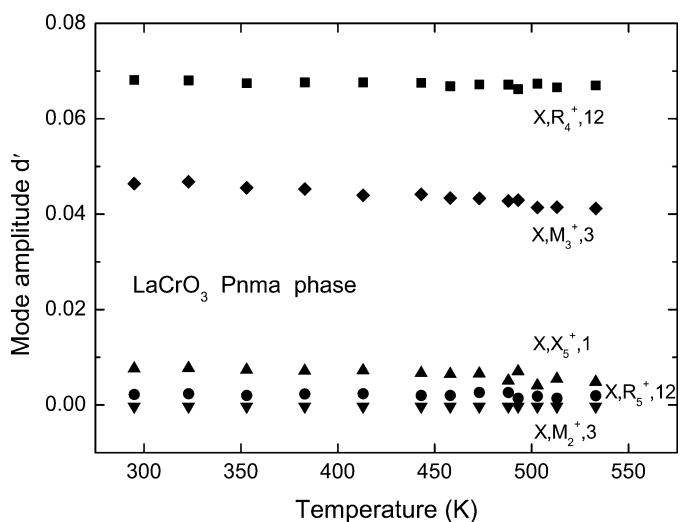

Figure 4
Variation of V_A/V_B with octahedral tilt-mode amplitudes $d_{X,M_3^+,3}$ and $d_{X,R_4^+,12}$ of the *Pnma* phase of LaCrO$_3$ perovskite. The surface is the $V_A/V_B(d_{X,M_3^+,3}, d_{X,R_4^+,12})$ expression for the *Pnma* structure given in Table 2(h).

Figure 5
Variation of the mode amplitudes $d_{X,M_2^+,3}$, $d_{X,M_3^+,3}$, $d_{X,R_4^+,12}$, $d_{X,R_5^+,12}$ and $d_{X,X_5^+,1}$ with temperature in the *Pnma* phase of LaCrO$_3$ perovskite.

three octahedral distortion mode amplitudes $d_{X,M_2^+,3}$, $d_{X,R_5^+,12}$ and $d_{X,X_5^+,1}$. The $d_{X,M_3^+,3}$, $d_{X,R_4^+,12}$ and V_A/V_B values calculated from the X-anion coordinates of $Pnma$ LaCrO$_3$ structures over the experimental temperature range are shown in the coordinate frame in Fig. 4. An enlargement and re-alignment of this surface in Fig. 6 shows that the experimental volume ratios are very close (typically within 0.002, but as much as 0.03 for the example of extremely distorted MgSiO$_3$ perovskite), but smaller than the ratios calculated from the contributions of the tilt modes alone. The fact that the actual volume ratios fall below the surface calculated for tilts alone is a typical case for the perovskites in this class, and indicates that the contribution of the terms in the triplets in the denominator is positive and larger in magnitude than the sum of the terms in the squares of $d_{X,M_2^+,3}$ and $d_{X,R_5^+,12}$. The opposite case occurs when there is a significant M_2^+ distortion, as typically occurs in compounds with Jahn–Teller distorted octahedra such as LaMnO$_3$ (*e.g.* Rodriguez-Carvajal *et al.*, 1998). In these cases the term in the square of $d_{X,M_2^+,3}$ outweighs the triplet terms and the true V_A/V_B becomes slightly larger (of the order of 0.01) than the value calculated from the amplitudes of the tilt modes alone.

Therefore, even in the presence of significant amplitudes of the distortional modes the octahedral tilt mode amplitudes play a dominant role in changing V_A/V_B because the distortional modes contribute at most a change of the order of 0.03 to the volume ratio, or typically less than 5% of the difference of V_A/V_B from 5. This is in agreement with the observation that the majority of 761 experimental $Pnma$ structures have V_A/V_B between 4.4 and 4.8 determined mostly by the tilting (Avdeev *et al.*, 2007). Returning to the example of $Pnma$ LaCrO$_3$ perovskite, we also note that it also displays the general trend that as temperature increases both the distortional and tilt modes show a decrease in amplitude and the deviation of the true V_A/V_B value from that calculated for the tilts alone becomes smaller (Fig. 6). So, as in real $Imma$ perovskites, for many practical purposes the contributions to the volume ratio from the distortional modes can be neglected.
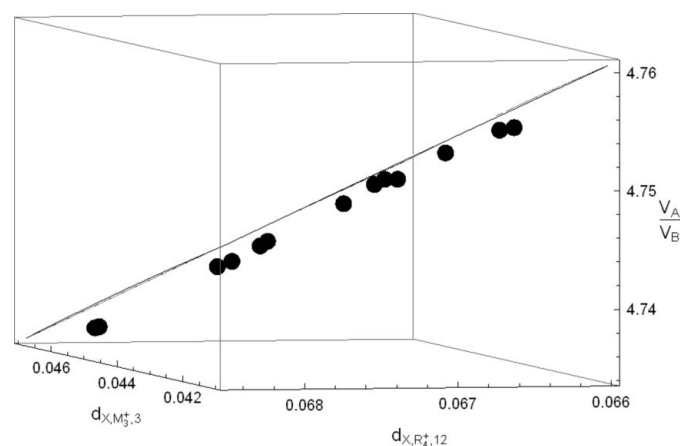
6. Conclusions

We have used the computer programs *ISOTROPY* and *ISODISTORT* to decompose perovskite structures in terms of symmetry-adapted displacive modes following the methodology of Knight (2009). With a new definition, $d' = d/a_p$, the mode amplitudes only reflect the internal degrees of freedom of the structure, and not the influence of the deformation of the cell parameters of the supercell away from those of the cubic parent structure. The polyhedral volume ratio V_A/V_B that defines whether a perovskite structure becomes more or less distorted with changes in pressure or temperature has been defined in terms of the mode amplitudes involving the X anions for each of 15 tilt systems. These expressions have been reduced to a simple universal form [equation (6)] applicable to all tilt systems by neglecting the octahedral distortion modes. V_A/V_B has also been obtained as a function of the tilt angles about the three pseudo-cubic axes [equation (8)]. The dominance of octahedral tilt modes over the distortional modes found in real perovskites justifies the use of the simple uniform expression for most cases.

Figure 6
The variation of V_A/V_B with octahedral tilt-mode amplitudes $d_{X,M_3^+,3}$ and $d_{X,R_4^+,12}$ of the $Pnma$ phase of LaCrO$_3$ perovskite replotted from Fig. 4 over a smaller range of mode amplitudes and oriented to view edge-on the surface of V_A/V_B ($d_{X,M_3^+,3}$, $d_{X,R_4^+,12}$) of $Pnma$ perovskites given in Table 2(*h*).

References

Andrault, D. & Poirier, J. P. (1991). *Phys. Chem. Miner.* **18**, 91–105.
Angel, R. J., Zhao, J. & Ross, N. L. (2005). *Phys. Rev. Lett.* **95**, 025503.
Avdeev, M., Caspi, E. N. & Yakovlev, S. (2007). *Acta Cryst.* B**63**, 363–372.
Avdeev, M., Seabra, M. P. & Ferreira, V. M. (2002). *Mater. Res. Bull.* **37**, 1459–1468.
Basyuk, T., Vasylechko, L., Fadeev, S., Syvorotka, I. I., Trots, D. & Niewa, R. (2009). *Rad. Phys. Chem.* **78**, S97–S100.
Campbell, B. J., Stokes, H. T., Tanner, D. E. & Hatch, D. M. (2006). *J. Appl. Cryst.* **39**, 607–614.
Carpenter, M. A. (2007). *Am. Mineral.* **92**, 309–327.
Carpenter, M. A., Howard, C. J., Kennedy, B. J. & Knight, K. S. (2005). *Phys. Rev. B*, **72**, 024118.
Carpenter, M. A., Sinogeikin, S. V. & Bass, J. D. (2010). *J. Phys. Condens. Matter*, **22**, 035404.
Cohen, R. E. (1992). *Nature*, **358**, 136–138.
Cowley, R. A. (1964). *Phys. Rev.* **134**, A981.
Darlington, C. N. W. (2002a). *Acta Cryst.* A**58**, 66–71.
Darlington, C. N. W. (2002b). *Acta Cryst.* A**58**, 299–300.
Dobson, D. P. & Jacobsen, S. D. (2004). *Am. Mineral.* **89**, 807–811.
Fu, W. T. & Ijdo, D. J. W. (2006). *J. Solid State Chem.* **179**, 2732–2738.
Fu, W. T., Visser, D. & Ijdo, D. J. W. (2005). *Solid State Commun.* **134**, 647–652.
Fu, W. T., Visser, D., Knight, K. S. & Ijdo, D. J. W. (2004). *J. Solid State Chem.* **177**, 1667–1671.

research papers

Fu, W. T., Visser, D., Knight, K. S. & Ijdo, D. J. W. (2007). *J. Solid State Chem.* **180**, 1559–1565.

Glazer, A. M. (1972). *Acta Cryst.* B**28**, 3384–3392.

Goodwin, A. L., Redfern, S. A. T., Dove, M. T., Keen, D. A. & Tucker, M. G. (2007). *Phys. Rev. B*, **76**, 174114.

Hashimoto, T., Tsuzuki, N., Kishi, A., Takagi, K., Tsuda, K., Tanaka, M., Oikawa, K., Kamiyama, T., Yoshida, K., Tagawa, H. & Dokiya, M. (2000). *Solid State Ionics*, **132**, 181–188.

He, T., Huang, Q., Ramirez, A. P., Wang, Y., Regan, K. A., Rogado, N., Hayward, M. A., Haas, M. K., Slusky, J. S., Inumara, K., Zandbergen, H. W., Ong, N. P. & Cava, R. J. (2001). *Nature*, **411**, 54–56.

Hofer, H. E. & Kock, W. F. (1993). *J. Electrochem. Soc.* **140**, 2889–2894.

Howard, C. J., Knight, K. S., Kennedy, B. J. & Kisi, E. H. (2000). *J. Phys. Condens. Matter*, **12**, L677–L683.

Howard, C. J. & Stokes, H. T. (1998). *Acta Cryst.* B**54**, 782–789.

Howard, C. J. & Stokes, H. T. (2002). *Acta Cryst.* B**58**, 565.

Howard, C. J. & Stokes, H. T. (2004). *Acta Cryst.* B**60**, 674–684.

Kennedy, B. J., Saines, P. J., Zhou, Q., Zhang, Z., Matsuda, M. & Miyake, M. (2008). *J. Solid State Chem.* **181**, 2639–2645.

Knee, C. S., Magraso, A., Norby, T. & Smith, R. I. (2009). *J. Mater. Chem.* **19**, 3238–3247.

Knight, K. S. (1994). *Solid State Ionics*, **74**, 109–117.

Knight, K. S. (2009). *Can. Mineral.* **47**, 381–400.

Liu, L. G. (1976). *Phys. Earth Planet. Int.* **11**, 289–298.

Macquart, R. B., Kennedy, B. J. & Avdeev, M. (2010). *J. Solid State Chem.* **183**, 249–254.

Malavasi, L., Ritter, C. & Chiodelli, G. (2008). *Chem. Mater.* **20**, 2343–2351.

Mao, H. K., Yagi, T. & Bell, P. M. (1977). *Carnegie Institution of Washington Year Book*, Vol. 76, pp. 502–504. Washington DC: Carnegie Institution.

Megaw, H. D. (1966). *Proceedings of the International Meeting on Ferrelectricity*, Vol. 1, edited by V. Dvorak, A. Fouskova & P. Glogar, pp. 314–321. Prague: Institute of Physics of the Czechoslovak Academy of Sciences.

Miller, S. C. & Love, W. F. (1967). *Tables of Irreducible Representations of Space Groups and Co-representations of Magnetic Space Groups*. Boulder, Colarado: Pruett.

Mountstevens, E. H., Attfield, J. P. & Redfern, S. A. T. (2003). *J. Phys. Condens. Matter*, **15**, 8315–8326.

Oikawa, K., Kamiyama, T., Hashimoto, T., Shimojyo, Y. & Morii, Y. (2000). *J. Solid State Chem.* **154**, 524–529.

Pagnier, T., Charrier-Cougoulic, I., Ritter, C. & Lucazeau, G. (2000). *Eur. Phys. J. Appl. Phys.* **9**, 1–9.

Perez-Mato, J. M., Orobengoa, D. & Aroyo, M. I. (2010). *Acta Cryst.* A**66**, 558–590.

Ranjan, R., Agrawal, A., Senyshyn, A. & Boysen, H. (2006). *J. Phys. Condens. Matter*, **18**, 9679–9690.

Reid, A. F. & Ringwood, A. E. (1975). *J. Geophys. Res.* **80**, 3363–3370.

Ringwood, A. E. (1962). *J. Geophys. Res.* **67**, 4005–4010.

Rodriguez-Carvajal, J., Hennion, M., Moussa, F., Moudden, A. H., Pinsard, L. & Revcolevschi, A. (1998). *Phys. Rev. B*, **57**, R3189–R3192.

Saines, P. J., Kennedy, B. J. & Smith, R. I. (2009). *Mater. Res. Bull.* **44**, 874–879.

Stokes, H. T., Hatch, D. M. & Campbell, B. J. (2007). *ISOTROPY*, http://stokes.byu.edu/isotropy.html.

Tamazyan, R. & van Smaalen, S. (2007). *Acta Cryst.* B**63**, 190–200.

Thomas, N. W. (1996). *Acta Cryst.* B**52**, 16–31.

Thomas, N. W. (1998). *Acta Cryst.* B**54**, 585–599.

Thomas, N. W. & Beitollahi, A. (1994). *Acta Cryst.* B**50**, 549–560.

Uher, C. (1990). *J. Supercond.* **3**, 337–389.

Woodward, P. M. (1997). *Acta Cryst.* B**53**, 32–43.

Zhang, Z., Lumpkin, G. R., Howard, C. J., Knight, K. S., Whittle, K. R. & Osaka, K. (2007). *J. Solid State Chem.* **180**, 1083–1092.

Zhao, J., Ross, N. L. & Angel, R. J. (2004). *Acta Cryst.* B**60**, 263–271.